IRIS AperTO

UNIVERSITÀ DEGLI STUDI DI TORINO

AperTO - Archivio Istituzionale Open Access dell'Università di Torino

Electronic and Geometrical Structure of Zn+Ions Stabilized in the Porous Structure of Zn-Loaded Zeolite H-ZSM-5: A Multifrequency CW and Pulse EPR Study

This is the author's manuscript

Original Citation:

Availability:

This version is available http://hdl.handle.net/2318/1651675 since 2017-12-13T11:33:50Z

Published version:

DOI:10.1021/acs.jpcc.7b04289

Terms of use:

Open Access

Anyone can freely access the full text of works made available as "Open Access". Works made available under a Creative Commons license can be used according to the terms and conditions of said license. Use of all other works requires consent of the right holder (author or publisher) if not exempted from copyright protection by the applicable law.

(Article begins on next page)

20 April 2024

UNIVERSITÀ DEGLI STUDI DI TORINO

***This is an author version of the contribution published on**:*
Questa è la versione dell'autore dell'opera:

*J. Phys. Chem. C, 121 (26), **2017**, doi: 10.1021/acs.jpcc.7b04289*

The definitive version is available at:
La versione definitiva è disponibile alla URL:
http://pubs.acs.org/doi/abs/10.1021/acs.jpcc.7b04289

Electronic and Geometrical Structure of Zn^+ Ions Stabilized in the Porous Structure of Zn-Loaded Zeolite H-ZSM-5: A Multifrequency CW and Pulse EPR Study

Elena Morra,[†] Gloria Berlier,[†] Elisa Borfecchia,[†,‡] Silvia Bordiga,[†,§] Pablo Beato,[‡] and Mario Chiesa[*,†]

[†]Department of Chemistry, NIS Centre, and INSTM Reference Center, University of Turin, Via Giuria 7, Turin 10125, Italy

[‡]Haldor Topsøe A/S, Kongens Lyngby 2800, Denmark

[§]Department of Chemistry, University of Oslo, 1033 Blindern, Oslo 0315, Norway

Abstract

Electron spin resonance and hyperfine sublevel correlation (HYSCORE) spectroscopy at X- and Q-band frequencies have been employed, in conjunction with X-ray absorption spectroscopy (XAS), to determine the geometric and electronic structure of Zn^+ ions in H-ZSM-5 zeolite. Zn^+ ions were generated by the direct exposure of dehydrated acid H-ZSM-5 to Zn vapors. The number of Zn^+ ions is found to increase substantially upon UV irradiation. A single EPR active species is detected, indicating a single site of adsorption, characterized by the presence of an Al^{3+} site, as revealed by superhyperfine interactions. The full g (g_x = 1.9951, g_y = 1.9984, g_z = 2.0015) and ^{27}Al |A| (A_x = 2.8, A_y = 2.7, A_z = 4.6) MHz tensors were resolved, allowing for a detailed description of the geometric and electronic structure of Zn^+ ions stabilized in the cages of H-ZSM-5 zeolite. The dispersion and nuclearity of Zn species formed during the sublimation/irradiation process was assessed by means of XAS spectroscopy, which indicates the absence of metal or metal oxide particles in a significant amount.

INTRODUCTION

The intense electrostatic fields within zeolites labyrinthine networks of regular channels and cavities provide the driving force for the spontaneous ionization of molecular species and metal atoms and the stabilization of unusual formal valence states, resulting in unique physical and chemical properties. On contact with dehydrated zeolites, guest metal atoms, introduced from the vapor phase, can be spontaneously ionized by the zeolite host lattice, leading to the stabilization of extra-lattice cations and excess electrons into the zeolite structure.[1] In a similar way, molecular species can spontaneously ionize, leading to long-lasting charge-separated states.[2,3]

Of the many cationic clusters reported to form in zeolites, the majority have been alkali metal species,[1,4] although heavy metals of group 12 (Zn, Cd, and Hg) have also been investigated in the past.[5−9] Recently, attention has been focused on zinc-modified zeolite materials prepared throughthe direct sublimation of metallic zinc, where the stabilization of unusual Zn^{2+}[10−12] and Zn^+[13,14] species in the zeolite cages has been reported, along with interesting catalytic properties.[15−17]

Unlike mercury, which has an extensive +1 oxidation state chemistry, zinc usually adopts the +2 oxidation state, with the monovalent oxidation state being very unusual. Apart from zeolite matrices, evidence of the formation of monovalent zinc has been reported in the form of a polyzinc $[Zn^+]_8$ cluster[18] and of dimeric diamagnetic Zn_2^{2+} ions in $ZnCl_2$/Zn glasses at high temperatures[19] and in organometallic compounds.[20] Even rarer is the observation of monomeric Zn^+ species.

Zn^+ is a paramagnetic ion with $3d^{10}$ $4s^1$ electronic configuration; therefore, electron paramagnetic resonance (EPR) spectroscopy, although often neglected, is uniquely informative in the study of these chemical species. Indeed, very detailed EPR studies are available for ZnH and ZnF molecular species trapped in rare gas matrixes at 4 K[21,22] In the case of Zn^+ in zeotype materials, conventional continuous-wave (CW) X-band EPR has been used for the identification of Zn^+ species, mainly as an analytical tool. The most direct evidence of the formation of isolated Zn^+ paramagnetic ions has been reported by Li et al. using ^{67}Zn (I = 5/2)-enriched Zn.[14] Upon UV irradiation of the ^{67}Zn loaded zeolite, a sextuplet EPR spectrum centered at g = 1.998 is observed, which directly proves the formation of monovalent Zn ions. Importantly the EPR spectrum of monomeric Zn^+ species is observed upon UV irradiation of the sample.

This has led to different explanations concerning the nature of the diamagnetic precursors, invoking the presence of delocalized (EPR silent) electrons in the zeolite framework,[23] the photoionization of zerovalent Zn atoms,[12] or the homolytic splitting of diamagnetic Zn^{2+} pairs.[24]

A detailed knowledge of the precise nature and behavior of monovalent Zn^{+} cations at the molecular level is, however, still lacking, and advances can be obtained by fully exploiting the wealth of information that can be extracted from a detailed EPR study of the isolated paramagnetic species. We have recently shown that modern pulsed EPR methodologies offer unique opportunities to monitor the local environment and the elementary processes occurring within the coordination sphere of paramagnetic transition-metal ions (TMIs) in heterogeneous catalysts.[25,26] In particular, so-called hyperfine techniques (HYSCORE and ENDOR) have proven extremely useful to elucidate the local topology of paramagnetic TMI containing heterogeneous catalysts by detecting electron−nuclear hyper-fine interactions with magnetically active nuclei in the first- or second-coordination sphere. In the case of aluminosilicate zeotype materials, framework Al nuclei (I = 5/2) have suitable magnetic properties for the investigation of long-range magnetic interactions by high-resolution EPR techniques, which provide direct access to specific binding sites and geometry of paramagnetic species. It is the purpose of this work to provide, by means of a multifrequency CW and pulse EPR approach, a detailed description of the local structural environment and associated structure−property relationships of paramagnetic Zn^{+} species in ZSM-5, complemented by X-ray absorption spectroscopy (XAS) to assess the dispersion of sublimated Zn into the zeolite.

EXPERIMENTAL SECTION

Sample Preparation. The Zn/ZSM-5 sample was prepared by in situ sublimation of metallic zinc on the protonated ZSM-5 zeolite. The H-ZSM-5 zeolite (Si/Al = 20, supplied by Haldor Topsøe) was dehydrated by thermal treatment at 673 K under dynamic vacuum (residual pressure $<10^{-4}$ mbar) for 2 h and calcined at 773 K in an O_2 atmosphere to remove spurious organic residues. The activated zeolite was exposed for 2 min to metallic zinc vapors generated in situ by heating a zinc metal bead at 673 K. The Zn vapor pressure at this temperature was 0.4 mbar.[27] The Zn-doped zeolite was subsequently irradiated in situ with UV/vis light for 80 min using a 1500 W xenon lamp (New Port Instruments).

EPR Characterization. X-band CW EPR spectra were recorded at 298 K on a Bruker EMX spectrometer (microwave frequency 9.46 GHz) equipped with a cylindrical cavity. A microwave power of 0.1 mW, a modulation amplitude of 0.08 mT, and a modulation frequency of 100 kHz were used. X- and Q-band pulse EPR experiments were performed at 60 and 298 K on a Bruker ELEXYS 580 EPR spectrometer (microwave frequency 9.76 and 33.7 GHz) equipped with a liquid-helium cryostat from Oxford. The magnetic field was measured by means of a Bruker ER035 M NMR gaussmeter. Electron-spin-echo (ESE) detected EPR experiments were performed with the pulse sequence $\pi/2-\tau-\pi-\tau-$echo. Pulse lengths $t_{\pi/2}$ = 16 ns and t_{π} = 32 ns, a τ value of 200 ns, and a 0.5 kHz shot repetition rate were used. Six-pulse hyperfine sublevel correlation experiments[28,29] were carried out with the extended pulse sequence $(\pi/2)_x-\tau_1-(\pi)_x-\tau_1-(\pi/2)_y-t_1-(\pi)_y-t_2-(\pi/2)_y-\tau_2-(\pi)_y-\tau_2-$echo, applying an eight-step phase cycle for eliminating unwanted echoes. The t_1 and t_2 time intervals were incremented in steps of 16 ns, starting from 100 to 3300 ns. Pulse lengths $t_{\pi/2}$ = 8 ns and t_{π} = 16 ns and a 0.33 kHz shot repetition rate were used.
For the ^{27}Al 6p-HYSCORE spectra, equal τ_1 and τ_2 values were employed, namely, $\tau_1 = \tau_2$ = 128 ns for X-band and $\tau_1 = \tau_2$ = 112 ns for Q-band frequency. For the ^{1}H X-band experiments several different interpulse delays ($\tau_1 = \tau_2$ = 102 ns, $\tau_1 = \tau_2$ = 128 ns, and τ_1 = 24 ns, τ_2 = 136 ns) were used to avoid blind-spot effects. The time traces of the HYSCORE spectra were baseline-corrected with a third-order polynomial, apodized with a Hamming window, and zero-filled. After 2D Fourier transformation, the absolute-value spectra were calculated. Spectra recorded with different τ values were added to eliminate blind-spot effects.
EPR and HYSCORE spectra were simulated using the Easyspin package.[30]

EDS and XAS Characterization. Both techniques were employed on the sample exposed to atmosphere, after the in situ sublimation and EPR measurements. Zn content (2.3 wt %) was determined by energy-dispersive X-ray spectroscopy (EDS), with a scanning electron microscope FEI Quanta 200 FEG-ESEM equipped with an EDAX EDS detector.

The XAS experiment was performed at BM31 (Swiss Norwegian Beamline, SNBL-II) of the European Synchrotron Radiation Facility (ESRF, Grenoble, France). X-ray absorption near-edge (XANES) and extended X-ray absorption fine structure (EXAFS) spectra were measured at the Zn K-edge in transmission mode on pelletized samples using a water- cooled flat Si [111] double-crystal monochromator, providing an intrinsic energy resolution of $\Delta E/E \approx 1.4 \times 10^{-4}$. To measure the incident (I_0) and transmitted (I_1) X-ray intensity, 30 cm length ionization chambers filled with a mixture of He and Ar were used. A Zn foil was measured simultaneously with a third ionization chamber (I_2) for energy calibration. Continuous scans were performed in the range (9400 − 10600) eV with an equidistant energy spacing of 0.25 eV; collection of one XAS spectrum required ca. 30 min. Sublimated Zn-ZSM-5 sample was measured under ambient conditions (RT, air). As reference materials, Zn metal foil, ZnO, and a 50 mM aqueous solution of $Zn(NO_3)_2$ were measured on the BM23 beamline of the ESRF, under the same conditions and using equivalent data acquisition protocols as described before. A Zn-ZSM-5 sample with the same Si/Al ratio, prepared by ion exchange (IE) (1.9 Zn wt %), was also measured as reference both under ambient conditions and after dehydration at 693 K in technical air flow, using a gas-flow setup based on the Microtomo reactor cell, as described elsewhere.[31,32]
XAS spectra for the Zn-ZSM-5 and for the relevant reference materials were aligned in energy employing the corresponding Zn metal foil spectra detected by the I_2 ionization chamber and normalized to unity edge jump using the Athena software from the Demeter package.[33] The extraction of the $\chi(k)$ functions was also performed using Athena program, and R-space EXAFS spectra were obtained by calculating the Fourier transform of the $k^2\chi(k)$ functions in the (2.5−12.0) $Å^{-1}$ k range.

RESULTS AND DISCUSSION

Exposure of thermally dehydrated H-ZSM-5 zeolite to Zn vapors leads to the appearance of a distinct CW-EPR signal centered at about g = 1.99, which is assigned to Zn^+ species in agreement with previous reports.[12−16] The signal (Figure 1a) is characterized by a multiline pattern due to the hyperfine interaction (*hfi*) to a nearby ^{27}Al (I = 5/2) nucleus, which is resolved for the first time.

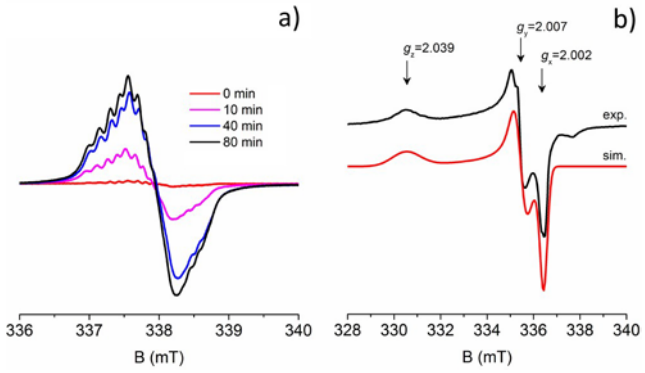

Figure 1. (a) X-band CW-EPR spectra recorded at room temperature of the ZSM-5 zeolite upon zinc sublimation and after different UV irradiating time. (b) X-band CW-EPR spectrum recorded at 77K upon reaction of the irradiated sample with 5 mbar of O_2.

The formation of Zn^+ species can be rationalized based on eq 1, considering the reduction of H^+ Brønsted sites, as proposed by Qi et al.[15] on the basis of MAS ^1H NMR data.

$$H^+ + Zn \rightarrow Zn^+ + \frac{1}{2}H_2 \qquad (1)$$

The EPR signal intensity increases of about one order of magnitude upon UV irradiation, indicating that EPR silent, diamagnetic precursors are converted into Zn^+ species upon irradiation. Such precursors have been suggested to be diamagnetic Zn_2^{2+} dimers, which undergo homolytic splitting upon UV irradiation (eqs 2 and 3).[24]

$$2H^+ + 2Zn \rightarrow Zn_2^{2+} + H_2 \quad (2)$$

$$Zn_2^{2+} + h\nu \rightarrow 2Zn^+ \quad (3)$$

The exact localization of the supposed dimer species is unclear at present and will be the object of future investigations. In this stage we limit ourselves to remark that the spectral features of the EPR spectrum do not change upon UV irradiation of the sample, indicating that all formed Zn^+ species are stabilized at the same "single-ion" active sites in the zeolite cages. It is the purpose of this work to investigate in detail the nature of such sites.

The formed Zn^+ species are indefinitely stable under vacuum but readily react via a one-electron transfer reaction, with oxygen leading to O_2^- ions, as demonstrated by the EPR spectrum reported in Figure 1b, which is consistent with previous reports.[15] Superior resolution over the more standard X-band frequency (9.5 GHz, Figure 2a) is obtained on recording the spectrum at the Q-band frequency (~34 GHz, Figure 2b). Because of the enhanced dominance of the Zeeman interaction (field dependent *g*-splitting) at this frequency, the g matrix anisotropy is resolved, resulting in a typical rhombic EPR powder pattern, with g_x = 1.9951, g_y = 1.9984, and g_z = 2.0015. Noticeably, each g matrix component is clearly split into a sextuplet of lines. This sextuplet structure is caused by the *hfi* of the Zn^+ unpaired electron with a nearby ^{27}Al nucleus (I = 5/2), as confirmed by 2D-HYSCORE experiments performed at Q-band (vide infra).

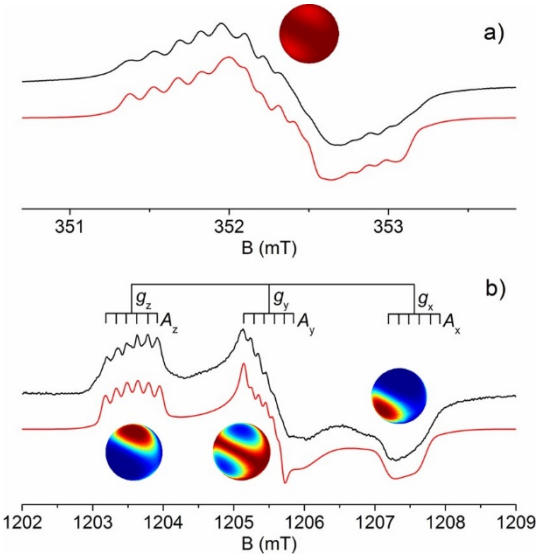

Figure 2. Experimental (black) and computer simulated (red) CW- EPR spectra of Zn^+/ZSM-5 recorded at (a) X-band (9.5 GHz) and (b) Q-band (34 GHz) frequencies. The stick diagram indicates the hyperfine coupling relative to the ^{27}Al nucleus (I = 5/2). The orientation selections on the unit spheres are shown for the observer positions of HYSCORE experiments.

The *g* values of Zn^+ ions in ZSM-5 are close to free-atom *g* value g_J = 2.0023, as it may be expected for a species possessing no orbital angular momentum (L = 0) with nominally states. In second-order perturbation theory the shift of the components of the g matrix from the free electron value is given by

$$\Delta g_{ij} = -2\lambda_{Zn}\Sigma_n <0|L_i|n><n|L_j|0>/(E_n - E_0) \quad (4)$$

where λ_{Zn} = 342 cm^{-1} is the Zn spin−orbit coupling constant, L_i are components of the angular momentum operator, 0 is the ground-state wave function (SOMO), and n is the wave function of the excited states. The observed experimental values can be accounted by a SOMO orbital (|0>) with a_1 symmetry, bearing mainly Zn^+ |4s> character with small admixture of |$4p_z$> orbital. Because of the symmetry restrictions, the matrix elements of L_z between the a_1 ground state and other states vanish, leading to a small departure of g_z from the free electron *g* value. On the contrary, the $L_{x,y}$ operator connects the ground state with |$p_{y,x}$> states, giving rise to the negative *g* shift in these directions. Thus $g_z > g_{y,x}$, consistent with the experimental g tensor. The observed

g values are also in line with data reported for ZnH[21] and ZnF[22] matrix isolated molecular radicals (Table 1) and for isoelectronic K atoms adsorbed on MgO.[34]

In line with the nominally perturbed $^2S_{1/2}$ ground state and the small *g* anisotropy, Zn^+ centers in ZSM-5 display remarkably long relaxation times at room temperature. A phase memory time T_m of 2 μs was measured at room temperature using the standard Hahn echo sequence, while T_1 of the order of 15 μs was measured with the inversion recovery sequence.

The rhombic g matrix clearly evidenced by the Q-band EPR spectrum calls for a low-symmetry site, which is expected if the Zn^+ is bound to oxygen bridges between silicon and aluminum atoms $[Si{-}O{-}Al]^-$ of the aluminosilicate framework, where its charge compensates for an acidic proton.

The presence of a single Al ion in the proximity of the Zn^+ center is demonstrated by the sextuplet hyperfine pattern in the CW EPR spectra (Figure 2). An improved resolution and the identity of the nucleus is obtained by means of orientationally selective six-pulse HYSCORE spectra at Q-band frequency (Figure 3a), which allow resolving the full set of electron − nuclear hyperfine interactions of the Zn^+ center with ^{27}Al framework ions.

Table 1. Spin-Hamiltonian Parameters for Zn^+ Species[a]

				^{27}Al			Ref
	g_x	g_y	g_z	A_x	A_y	A_z	
Zn/ZSM-5	1.9951	1.9984	2.0015	3.1	3.2	4.2	This work
ZnH	1.996		2.002				21
ZnF	1.9855		2.0003				22

[a]Hyperfine values are in megahertz

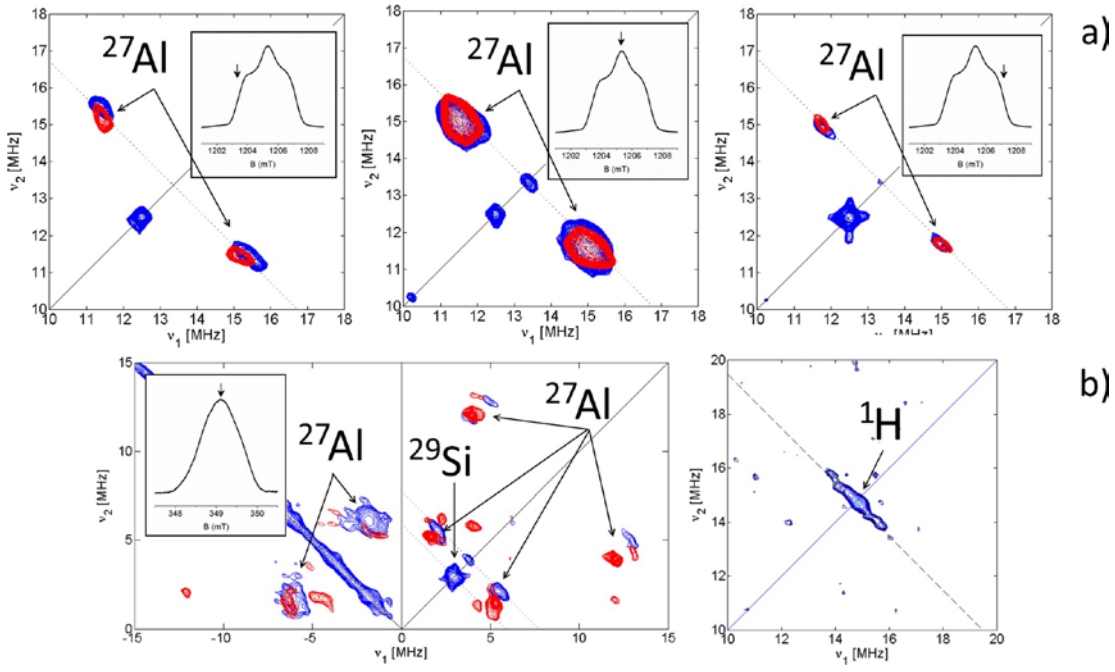

Figure 3. (a) Orientationally selective Q-band 6p-HYSCORE spectra recorded at the EPR spectrum turning points. The magnetic field setting is indicated for each spectrum. (b) X-band 6p-HYSCORE experiment recorded at the maximum echo intensity. Blue, experimental; red, simulated spectra. All spectra were recorded at room temperature. The ^1H HYSCORE spectrum is plotted separately at lower contour levels. For the simulation of the X-band spectrum the full powder orientation has been assumed. The following parameters were employed for all the simulations: g= [1.9951 1.9984 2.0015], A = [2.8 2.7 4.6] MHz, e^2qQ/h = 9 MHz, η = 1, α = 20°, β = 10°, γ = 90°, α′ = 50°, β′ = 90°, γ′ = 20°. An example of an alternative simulation ($|e^2qQ/h|$ = 12 MHz, η = *0.9*) is reported as Supporting Information.

Six-pulse HYSCORE spectra give substantially enhanced peak intensities for weakly modulating nuclei, as in the case of Q-band measurement of hyperfine interactions characterized by a small anisotropic component, and

were therefore used as an alternative to standard HYSCORE experiments. Thanks to the low relaxation rates of Zn^+ species, experiments were performed at room temperature at the EPR turning points and show well-resolved correlation peaks in the (++) quadrants, centered at the ^{27}Al nuclear Larmor frequency. ^{27}Al is a I = 5/2 nucleus with g_n = 1.4566, which means that the two-electron spin manifolds α (m_s = 1/2) and β (m_s = −1/2) will split into six levels according to the nuclear spin quantum numbers, which range from m_I = 5/2 to m_I = −5/2. In general, because of the nuclear quadrupole interaction these levels will be shifted proportionally to $(m_I)^2$. The HYSCORE spectrum for such a system will consist theoretically of $2(2I)^2$ = 50 correlation peaks for the $|\Delta m_I| = 1$ transitions and a number of cross peaks corresponding to $|\Delta m_I| = 2,3$ and so on. The transition frequencies of ^{27}Al between the states with the nuclear spin projections $m_I = +1/2$ and $m_I = -1/2$ are those least affected by the nuclear quadrupole interaction (*nqi*).

Therefore, these transitions are the most intense ones, and their frequencies are approximately (to first order in *hf i* and *nqi*) given by $\nu = \nu_I \pm A/2$, where ν_I is the ^{27}Al Zeeman frequency and A is the hyperfine coupling. The observation of two well- resolved off-diagonal cross peaks indicates that the hyperfine interaction with aluminum nuclear spins is dominated by the Fermi contact term. Computer simulation of the CW-EPR and Q-band HYSCORE spectra allowed extracting the ^{27}Al *hf i* parameters, reported in Table 1. Analysis of the hyperfine tensor indicates that the isotropic *hf i* constant is approximately ±3.4 MHz, while the anisotropic *hf i* constant is on the order of 0.6 MHz. An estimate of the ^{27}Al *nqi* parameters was obtained by simulating the X-band HYSCORE spectrum (Figure 3b). At this frequency, a number of multiple quantum transitions is observed in both quadrants, which can be explained by the effect of the nuclear quadrupole coupling. The simulation was carried out by keeping fixed the *hf i* values extracted from Q- band experiments and adjusting the *nqi* coupling tensor and its orientations relative to the *hf i* tensor until a satisfactory fit was achieved. A qualitative agreement between simulated and experimental spectra could be obtained with *nqi* values $|e^2qQ/h|$ ranging in the interval 9−12 MHz and an asymmetry parameter η in the interval 0.7 to 1. The simulations proved to be insufficiently sensitive to achieve a more accurate determination of the *nqi* parameters, as a qualitative fit of the experimental spectrum could be achieved with different values in this range (see Supporting Information). All simulations reported in Figures 2 and 3 were performed using the same set of spin- Hamiltonian parameters reported in the caption of Figure 3.

The obtained *nqi* parameters are consistent with the quadrupolar interaction of framework aluminum ions in dehydrated H-ZSM-5, for which $|e^2qQ/h|$ values in the interval 13−16 MHz have been reported.[35] The slightly smaller values extracted from the X-band HYSCORE spectra can be rationalized considering the lower polarization effect of Zn^+ with respect to H^+ and the consequent smaller electric field gradient. A signal at the ^{29}Si Larmor frequency is also clearly observed (Figure 3b) due to the hyperfine coupling with remote (matrix) ^{29}Si nuclei. Because the natural abundance of ^{29}Si is small (4.68%) the detection of directly coupled Si ions, in the proximity of Zn^+ ions, is hampered by sensitivity issues. Finally, a weak ^1H signal due to residual protons could be observed, which is shown in Figure 3b. The signal was observed after long accumulation time (24 h) and has a maximum extension of 2 MHz. Assuming a pure dipolar interaction, this translates into a minimum Zn^+−H^+ distance on the order of 0.43 nm. The low signal intensity can be associated with a relatively low number of residual protons after Zn evaporation (in line with the general formation mechanism of eq 1), combined with possible suppression effects of the ^1H HYSCORE signal due to ^{27}Al modulations.

The ^{27}Al HYSCORE experiments together with the Q-band CW EPR spectra allow ascertaining with accuracy the presence of a single Al ion in the second coordinative shell of the Zn^+ center. The absence of protons in the first coordination sphere, revealed by ^1H HYSCORE spectra, is further proof that Zn^+ substitute for acidic protons, which are presumably reduced during the process of metal evaporation. This is consistent with 1H MAS NMR spectra reported by ref 15, which show that proton Brønsted sites are consumed upon reaction with Zn.

The presence of a sizable isotropic hyperfine coupling indicates a direct bonding of the Zn^+ ions to the framework with significant spin density at the Al nucleus. Considering the value of a_0 = 3367.76 MHz for unit spin density on the ^{27}Al 3s orbital,[36] the corresponding spin density in the Al 3s orbital is ∼0.10%, in line with the spin transfer observed for para-magnetic TMIs (V^{4+}, Cu^{2+}) to second-shell Al^{3+} ions in zeotype materials.[37−40]

Taking into account that the unpaired electron mainly resides in the Zn 4s orbital (vide supra), the overlapping with the oxygen framework orbitals leads to a spin density transfer to the Al and Si framework nuclei, demonstrating the Zn^+- framework interaction and revealing a non-negligible degree of covalency in the bond structure. The high spectral resolution, absence of multiple species, and long relaxation times indicate that isolated monomeric paramagnetic Zn^+ species are stabilized at very specific single sites, next to an Al ion, as illustrated in Scheme 1. Recent DFT model structures[24] suggest a Zn−Al distance of 2.88 Å, which is compatible with the present results.

Scheme 1. Illustration of the Zn^+ Binding Site As Emerging from the Analysis of the EPR Experimental Data[a]

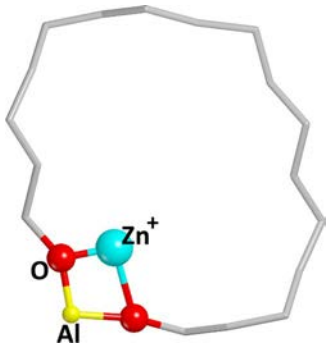

[a]Remote protons are not indicated.

Because EPR technique is sensitive only to paramagnetic species (in this context: isolated Zn^+ ions), it is important to employ complementary techniques to obtain information also about the general features of the Zn species (including the EPR-silent ones) inserted into the zeolite channels by in situ sublimation. To this aim, the sample recovered after the EPR measurements described above, was opened to atmosphere and measured as such by XAS at the Zn K-edge. This technique is element-sensitive, thus giving an averaged picture of all Zn species present in the sample.

The XANES and EXAFS spectra of the sublimated Zn-ZSM- 5 sample prepared and studied in this work are reported in Figure 4a,b, respectively. To facilitate the interpretation of these data, XAS spectra for a series of reference samples are also reported. Namely, these are Zn metal foil, ZnO and an aqueous solution of $Zn(NO_3)_2$ as a reference for hydrated Zn^{2+} ions. Moreover, the spectra obtained on a Zn-ZSM-5 zeolite with the same Si/Al ratio, prepared by IE of Zn^{2+} ions, are also reported (dotted curves). This has been measured both under ambient conditions and at 693 K in air flow, as a reference for dehydrated Zn^{2+} ions. No EPR spectra amenable to Zn^+ centers were observed in the IE-prepared Zn-ZSM-5 samples.

The XANES spectrum of sublimated Zn-ZSM-5 is easily assigned to divalent zinc ions (Figure 4a, thick black curve, edge position at 9663.1 eV, determined from the first maximum in the derivative of the $\mu x(E)$ curve and characteristic of Zn^{2+} centers).[41,42] This is not surprising because the Zn^+ ions formed in situ during Zn-metal sublimation are highly reactive and are readily oxidized, through the formation of superoxide ions, upon exposure to atmospheric conditions (see Figure 1b). However, this experiment was important to assess the dispersion and nuclearity of EPR-silent Zn species, possibly formed during the sublimation/irradiation process in addition to the EPR-active Zn+ species characterized above and persisting in the zeolite framework also under ambient conditions. Concerning nuclearity, we can safely exclude the presence of both metal Zn and ZnO particles, in a significant amount. Indeed, both bulk compounds are characterized by peculiar XANES features in the edge, white-line, and postedge regions, which are completely absent in the spectrum of sublimated Zn-ZSM-5 (compare thick black curve with green and gray ones in Figure 4a). Moreover, EXAFS spectra of the bulk compounds (Figure 4b, same color code) show intense peaks above 2.0 Å deriving from high-amplitude Zn−Zn single scattering paths, which are not observed on the Zn-sublimated sample. Namely, metal Zn is characterized by a first-shell Zn− Zn peak at ∼2.3 Å, while ZnO shows an intense second shell peak at ∼2.9 Å.

Additional considerations about the average Zn-speciation in the sublimated Zn-ZSM-5 sample measured in air are about the Zn ion hydration state. With this regard, it is interesting to compare the XAS spectra of Zn-

ZSM-5 to those of reference samples representative of hydrated Zn^{2+}, including $Zn(NO_3)_2$ aqueous solution, and IE Zn-ZSM-5 sample measured at room temperature in air (Figure 4, solid light-blue and dashed blue curves, respectively).

First, all hydrated samples are characterized by an intense white line, in agreement with the expected high coordination number of Zn^{2+} ions when solvated, occurring as Jahn−Teller distorted octahedral $[Zn^{2+}(H_2O)_6]^{2+}$ complexes.[41] The intensity of the white line decreases in the order hydrated Zn^{2+} > Zn-ZSM-5 IE > Zn-ZSM-5. The same order of intensity is observed in the first-shell EXAFS peaks at 1.5 to 1.6 Å, related to Zn−O coordination (Figure 4b). Accordingly, the intensity of the white line and EXAFS first shell peak of dehydrated Zn-ZSM-5 IE, also reported in Figure 4 (red dashed curves) for comparison, are considerably smaller. The coordination state of counterions in zeolites, when exposed to atmospheric moisture, is expected to be very similar to that of the same ions in aqueous solution, as observed in Cu-zeolites.[32] A lower average first-shell coordination number of Zn^{2+} (testified by the white-line and first-shell EXAFS peak intensity) in hydrated zeolites with respect to aqueous solution could suggest that a fraction of the Zn^{2+} sites is not accessible to water interaction. Indeed, it is interesting to notice that the XANES spectrum of Zn-ZSM-5 is intermediate between the ones of hydrated and dehydrated IE Zn-ZSM-5. Also, the EXAFS first shell peak of Zn-ZSM-5 is closer in position to dehydrated Zn-ZSM-5 IE than to the hydrated references (~2.5 vs ~2.6 Å).

All of these observations, taken together, indicate that the dispersion of zinc in the sublimated sample is high but not equal to what was obtained by IE, where one would suppose that Zn^{2+} ions are mainly present as counterions. A minor fraction of zinc ions could be present as very small or structurally disordered clusters (with broad Zn−Zn distance distributions), hence escaping detection by EXAFS. These could resist rehydration under ambient conditions, thus accounting for a XAS signature not fully equivalent to hydrated Zn^{2+} references, both in solution and in the conventional IE Zn-ZSM-5 samples. This general picture is in agreement with EPR interpretation discussed above and literature reports[12,17] proposing the formation of dimeric or slightly bigger clusters upon sublimation.

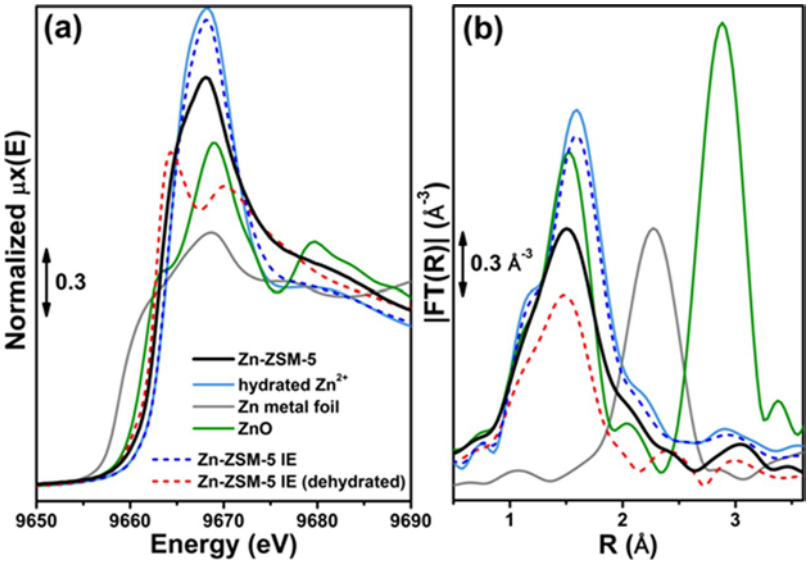

Figure 4. (a) XANES and (b) phase-uncorrected FT-EXAFS spectra of the sublimated Zn-ZSM-5 sample studied in this work measured under ambient conditions (room temperature, air). For comparison, XAS spectra for a selection of relevant Zn^0 and Zn^{2+} reference samples are reported.

CONCLUSIONS

A combination of CW-EPR and HYSCORE spectroscopies at X- and Q-band frequencies, supplemented by XAS spectroscopy, was used to characterize the local environment of isolated Zn^+ "single-ion" active sites localized within the cages of Zn loaded H-ZSM-5 zeolites. EPR spectroscopy indicates that a small fraction of paramagnetic isolated Zn^+ ions are formed upon direct contact of Zn vapors with the dehydrated zeolite. The number of these species increases by approximately one order of magnitude upon UV irradiation, indicating

the presence of diamagnetic precursors. XAS spectroscopy confirms the absence of EPR-silent metal or metal oxide particles in a significant amount, supporting the formation of large fractions of Zn_2^{2+} dimeric diamagnetic species upon sublimation. Such species, which will be the focus of future investigations, may act as diamagnetic precursors of the paramagnetic Zn^+ species, which are formed upon UV irradiation. Hyperfine interactions of the Zn^+ ions with a framework Al nucleus are resolved for the first time, providing the first direct experimental evidence of the localization of Zn^+ ions in proton-free cavities and preferential interaction with the Al^{3+} cation. The determined spin-Hamiltonian parameters provide detailed reference data and constraints for DFT calculations, which can be used to recover an atomic-level description of the site. To conclude, we have shown that advanced EPR techniques provide a detailed picture of the spatial and electronic structure of exotic Zn^+ sites in dehydrated zeolite H-ZSM-5, clearly emphasizing the role of the topology of the zeolite catalyst and, in particular, of framework Al sites in driving the reaction pathway and the stabilization of reactive species.

AUTHOR INFORMATION

Corresponding Author
*E-mail: mario.chiesa@unito.it.
ORCID
Elisa Borfecchia: 0000-0001-8374-8329
Silvia Bordiga: 0000-0003-2371-4156
Mario Chiesa: 0000-0001-8128-8031

Notes

The authors declare no competing financial interest.

ACKNOWLEDGMENTS

We thank M. Morteń and M. Mykland from Department of Chemistry, University of Oslo for EDS analysis. We are grateful to M. Brunelli (beamline BM31), and M. Monte Caballero, D. Motta Meira and K. A. Lomachenko (beamline BM23) for the support during XAS data collection at the ESRF. I. Pankin (IRC “Smart Materials”, Southern Federal University, Rostov-on- Don, Russia) is also acknowledged for XAS measurements at BM31.

REFERENCES

(1) Edwards, P. P.; Anderson, P. A.; Thomas, J. M. Dissolved Alkali Metals in Zeolites. *Acc. Chem. Res.* 1996, *29*, 23−29.
(2) Moissette, A.; Vezin, H.; Gener, I.; Patarin, J.; Bremard, C. Electron-Hole Pairs Stabilized in Al-ZSM-5. *Angew. Chem., Int. Ed.* 2002, *41*, 1241−1244.
(3) Moissette, A.; Hureau, M.; Col, P.; Vezin, H. Electron Transfers in Donor−Acceptor Supramolecular Systems: Highlighting the Dual Donor and Acceptor Role of ZSM-5 Zeolite. *J. Phys. Chem. C* 2016, *120*, 17372−17385.
(4) Rabo, J. A.; Angell, C. L.; Kasai, P. H.; Schomaker, V. Studies of Cations in Zeolites: Adsorption of Carbon Monoxide; Formation of Ni Ions and Na3+4 Centres. *Discuss. Faraday Soc.* 1966, *41*, 328−349.
(5) Zhen, S.; Bae, D.; Seff, K. Zn^+ Cations, Probable Tl_4Zn_{12} and Tl_6 Clusters, and Zeolite Desilication (Less Likely Dealumination): Crystallographic Study of the Incomplete Reaction of Zn Vapor with Tl^+-Exchanged Zeolite X. *J. Phys. Chem. B* 2000, *104*, 515−525.
(6) Readman, J. E.; Barker, P. D.; Gameson, I.; Hriljac, J. A.; Zhou, W.; Edwards, P. P.; Anderson, P. A. An Ordered Array of Cadmium Clusters Assembled in Zeolite A. *Chem. Commun.* 2004, *6*, 736−737.
(7) Choi, E. Y.; Lee, S. H.; Kim, Y.; Han, Y. W.; Seff, K. Crystal Structure of a Cadmium Sorption Complex of Dehydrated Fully Cd^{2+}- Exchanged Zeolite X Containing Cd^{2+}, Cd^+, and Cd^0. *J. Phys. Chem. B* 2002, *106*, 7569−7573.
(8) Barrer, R. M.; Whiteman, J. L. Mercury Uptake in Various Cationic Forms of Several Zeolites. *J. Chem. Soc. A* 1967, 19−25.
(9) Wang, J.-F.; Wang, D.; Zeng, H.; Zhou, Z.-F. Preparation and Oxygen Storage of Cadmium-modified Zeolites with Superior Electron Transfer Capacities. *RSC Adv.* 2015, *5*, 77490−77494.

(10) Seidel, A.; Rittner, F.; Boddenberg, B. Chemical Vapor Deposition of Zinc in Zeolite HY. *J. Phys. Chem. B* 1998, *102*, 7176−7182.
(11) Seff, K. Comment on ″Synthesis of Fully Dehydrated Fully Zn^{2+}-exchanged Zeolite Y and its Crystal Structure Determined by Pulsed-neutron Diffraction″. Cationic Zinc Clusters Formally Containing Zn(I) in the Sodalite Cavities of Zeolite Y (FAU). *J. Phys. Chem. B* 2005, *109*, 13840−13841.
(12) Oda, A.; Ohkubo, T.; Yumura, T.; Kobayashi, H.; Kuroda, Y. Synthesis of an Unexpected $[Zn_2]2+$ Species Utilizing an MFI-type Zeolite as a Nano-reaction Pot and its Manipulation with Light and Heat. *Dalton Trans.* 2015, *44*, 10038−10047.
(13) Oda, A.; Torigoe, H.; Itadani, A.; Ohkubo, T.; Yumura, T.; Kobayashi, H.; Kuroda, Y. Success in Making Zn^+ from Atomic Zn^0 Encapsulated in an MFI-Type Zeolite with UV Light Irradiation. *J. Am. Chem. Soc.* 2013, *135*, 18481−18489.
(14) Li, L.; Li, G.-D.; Yan, C.; Mu, X.-Y.; Pan, X.-L.; Zou, X.-X.; Wang, K.-X.; Chen, J.-S. Efficient Sunlight-Driven Dehydrogenative Coupling of Methane to Ethane over a Zn^+-Modified Zeolite. *Angew. Chem., Int. Ed.* 2011, *50*, 8299−8303.
(15) Qi, G.; Xu, J.; Su, J.; Chen, J.; Wang, X.; Deng, F. Low-Temperature Reactivity of Zn+ Ions Confined in ZSM-5 Zeolite toward Carbon Monoxide Oxidation: Insight from in Situ DRIFT and ESR Spectroscopy. *J. Am. Chem. Soc.* 2013, *135*, 6762−6765.
(16) Chen, G.; Zhao, Y.; Shang, L.; Waterhouse, G. I. N.; Kang, X.;Wu, L.-Z.; Tung, C.-H.; Zhang, T. Recent Advances in the Synthesis, Characterization and Application of Zn^+-containing Heterogeneous Catalysts. *Adv. Sci.* 2016, *3*, 1500424.
(17) Xu, J.; Zheng, A.; Wang, X.; Qi, G.; Su, J.; Du, J.; Gan, Z.; Wu, J.; Wang, W.; Deng, F. Room Temperature Activation of Methane over Zn Modified H-ZSM-5 Zeolites: Insight from Solid-state NMR and Theoretical Calculations. *Chem. Sci.* 2012, *3*, 2932−2940.
(18) Cui, P.; Hu, H.-S.; Zhao, B.; Miller, J. T.; Cheng, P.; Li, J. A Multicentre-bonded $[ZnI]_8$ Cluster with Cubic Aromaticity. *Nat. Commun.* 2015, *6*, 6331−5.
(19) Kerridge, D. H.; Tariq, S. A. The Solution of Zinc in Fused Zinc Chloride. *J. Chem. Soc. A* 1967, 1122−1125.
(20) Resa, I.; Carmona, E.; Gutierrez-Puebla, E.; Monge, A. Decamethyldizincocene, a Stable Compound of Zn(I) with a Zn-Zn Bond. *Science* 2004, *305*, 1136−1138.
(21) Knight, L. B.; Weltner, W. Hyperfine Interaction, Chemical Bonding, and Isotope Effect in ZnH, CdH, and HgH Molecules. *J. Chem. Phys.* 1971, *55*, 2061−2070.
(22) Knight, L. B.; Mouchet, A.; Beaudry, W. T.; Duncan, M. High-temperature Generation and ESR Matrix Isolation Studies of ZnF and CdF in Neon and Argon Matrices. *J. Magn. Reson.* 1978, *32*, 383−390.
(23) Wang, J. F.; Wang, K. X.; Wang, J. Q.; Li, L.; Jiang, Y. M.; Guo, X. X.; Chen, J. S. Elucidation of the chemical Environment for Zinc Species in an Electron-Rich Zinc-Incorporated Zeolite. *J. Solid State Chem.* 2013, *202*, 111−115.
(24) Benco, L. Electronic Structure of Zn^+-Modified Zeolite: A Density Functional Theory Study of Ferrierite. *J. Phys. Chem. C* 2016, *120*, 6031−6038.
(25) Maurelli, S.; Vishnuvarthan, M.; Chiesa, M.; Berlier, G.; Van Doorslaer, S. Elucidating the Nature and Reactivity of Ti Ions Incorporated in the Framework of AlPO4−5 Molecular Sieves. New Evidence from 31P HYSCORE Spectroscopy. *J. Am. Chem. Soc.* 2011, *133*, 7340−7343.
(26) Morra, E.; Giamello, E.; Chiesa, M. EPR Approaches to Heterogeneous Catalysis. The Chemistry of Titanium in Heteroge- neous Catalysts and Photocatalysts. *J. Magn. Reson.* 2017, *280*, 89− 102.
(27) *Handbook of Chemistry and Physics*, 76th ed.; CRC Press: Boca Raton, FL, 1995/1996, Section 6, 111.
(28) Song, R.; Zhong, Y. C.; Noble, C. J.; Pilbrow, J. R.; Hutton, D. R. A New Six Pulse Two-dimensional Electron Spin Echo Envelope Modulation (ESEEM) Correlation Spectroscopy. *Chem. Phys. Lett.* 1995, *237*, 86−90.
(29) Kasumaj, B.; Stoll, S. 5- and 6-pulse Electron Spin Echo Envelope Modulation (ESEEM) of Multi-nuclear Spin Systems. *J. Magn. Reson.* 2008, *190*, 233−247.
(30) Stoll, S.; Schweiger, A. EasySpin, a Comprehensive Software Package for Spectral Simulation and Analysis in EPR. *J. Magn. Reson.* 2006, *178*, 42−55.